metals

MDPI

Article

Development of an Instrumented Test Tool for the Determination of Heat Transfer Coefficients for Die Casting Applications

Yosra Kouki *, Sebastian Müller, Torsten Schuchardt and Klaus Dilger

Institute of Joining and Welding, Technische Universität, 38106 Braunschweig, Germany; sebastian.mueller@tu-braunschweig.de (S.M.); t.schuchardt@tu-braunschweig.de (T.S.); k.dilger@tu-braunschweig.de (K.D.)

* Correspondence: y.kouki@tu-braunschweig.de; Tel.: +49-(0)-531-391-95522

Received: 26 June 2020; Accepted: 14 August 2020; Published: 8 September 2020

Abstract: In the case of casting processes with permanent molds, there is still a relatively pronounced lack of knowledge regarding the locally prevailing heat transfer between casts and mold. This in turn results in an insufficient knowledge of the microstructure and the associated material properties in the areas of the casting component close to the surface. Therefore, this work deals with the design and evaluation of a test tool with an integrated sensor system for temperature measurements, which was applied to obtain a time-dependent heat transfer coefficient (HTC) during casting solidification. For this purpose, the setup, design and computational approach are described first. Special attention is paid to the qualification of the multi-depth sensor and the calculation method. For the calculations, an inverse estimation method (nonlinear sequential function) was used to obtain the HTC profiles from the collected data. The developed sensor technology was used in a test mold to verify the usability of the sensor technology and the plausibility of the obtained calculation results under real casting conditions and associated temperature loads. Both the experimental temperature profiles and the HTC profiles showed that, in the evaluated casting series, the peak values determined were close to each other and reached values between 6000 W/(m^2·K) and 8000 W/(m^2·K) during solidification.

Keywords: HPDC; test tool; integrated sensor system; HTC; inverse method; multi-depth temperature sensor; instrumented mold

1. Introduction

In terms of high production and material efficiency, die casting processes are very suitable manufacturing processes for the mass production of components with a high geometric complexity. This is particularly true for industrial sectors in which the challenge of reducing component weight while at the same time achieving very good quality and high strength of the parts is becoming increasingly important. Simultaneously, the use of light metals is also becoming increasingly important in this area.

The final quality of the cast components depends on various process and thermophysical parameters [1]. Recently, many efforts have been made [2–5] to integrate advanced sensor technologies into the permanent mold casting process. In addition to a better understanding of the process behavior, advanced sensor technology has also enabled us to monitor and control various casting parameters. The aim was to achieve an improved casting process that was optimized with regard to criteria such as energy consumption and final quality of the cast components. Some studies have already presented special sensors that were embedded in the die casting process and were able to withstand the harsh process conditions during the entire manufacturing process [5].

In the literature [6–8], it has been shown that the quality of the castings is strongly influenced by the solidification phase and the associated local cooling rates of the melt. The locally prevailing cooling rates control the microstructure development and the associated mechanical and technological component properties, for example, the size and distribution of the pores [9]. The cooling rate in turn depends, among other factors, on the heat transfer coefficient between the cast component and the casting die, which characterizes the thermal resistance between melt and die surface [10]. Further process parameters are, for example, the surface temperature, the temperature control system and the materials and coatings used in the die. In order to predict and optimize the quality of the casting products prior to production start and to reduce production risks, the use of casting simulation is widespread. However, the accuracy of the simulation results is linked to a sufficiently precise knowledge of the various boundary conditions and parameters of the casting process. In contrast to the above mentioned further process influencing parameters, the heat transfer coefficient is very dynamic and locally variable in its temporal development. Numerous models have been proposed to predict and determine the HTC for casting applications. Hamasaiid et al. [11] have introduced an interesting work in which an analytical model in the aim to predict the HTC for die casting processes was presented. Different parameters are integrated into this model, such as casting process parameters, the used die characteristics, and the thickness. As a result, the model was able to predict on the one hand the function of the HTC and on the other hand the effect of the various used parameters on the HTC. Other researchers and industrialists also validated the model in other processes, such as plastic injection molding. Vasileiou et al. [12] developed an approach based on the use of a genetic algorithm and numerical simulation for the determination of the local heat transfer coefficient in precision casting. For the method mentioned above, the retrieved HTC values were used for simulation and the numerically resulting cooling curves were compared to the experimental ones until the best match was found to affirm the HTCs determined values. Recently, Aksoy and Koru [13] used artificial intelligence methods to estimate the HTC in pressure die casting for aluminum alloys. The DTR, MLR, and ANNR learning algorithms, based on process parameters (casting temperature, injection pressure, and injection speed), were evaluated. As a result, the ANNR algorithm showed the best estimation accuracy of 99.9%.

Currently, there is no established method in casting simulation to use the local gap formation during solidification to calculate a time-dependent heat transfer coefficient. However, based on previous research, a time-dependent HTC can be determined locally by using an inverse method that is more accurate than other techniques [14]. The inverse method is based on the temperature measurement of the die and the melt during the casting process. A high accuracy of the temperature history is required, since every small temperature error can result in a high deviation of the reconstructed HTC value. Dour et al. [15] mentioned that these errors are mainly related to the configuration of the temperature sensors used. The main preventive measures that should be taken in the instrumentation are: the arrangement of the sensors, with the first thermocouple as close as possible to the surface of the die, and a fast response of the sensors. In this context, the present work introduces an instrumented test tool in which a specially developed multi-depth temperature sensor has been embedded for direct measurement of the die temperature during the casting process. The designed sensor offers numerous advantages in terms of manufacturing and application. For example, the developed method enables a simple and cost-effective production of the sensors, so that it also seems realistic from an economic point of view to use numerous sensors in a single mold. Along with the relatively compact, standardized design, this makes it possible to measure the solidification behavior of various areas of the casting and to obtain more comprehensive information about the relationship between process properties and component quality. Furthermore, it can be used in different industrial applications, as it has shown reliable and robust measurements during the evaluation and validation steps in this work. In addition, a two-color pyrometer was integrated, which allowed the measurement of the surface temperature of the melt in real time. An additional displacement sensor was also embedded in this test tool, which allowed a better understanding of the shrinkage of the casting by measuring the gap formed between the cavity and the casting during solidification. In this paper, however, the focus is only on measuring the temperature of the mold and the casting in order to reconstruct the heat transfer coefficient. More attention was paid to the design, calibration, and validation of the MDTS in a novel concept. With the help of a data acquisition system, it was possible to measure both temperatures simultaneously in real time at high frequency. Based on the collected temperature data, the so-called Beck's reversal method was used to determine the interface HTC between the casting made of an AlSi10Mg alloy and an H11 steel mold. The experiments were carried out as a preliminary test for the real application in a real die casting process.

2. Methodology

In order to achieve the overall goal of a valid determination of the heat transfer coefficient, the necessary work was divided into individual research tasks. In this context, Figure 1 shows the approach and the individual tasks performed. In the first stage (preparation), a suitable method for estimating the HTC, the nonlinear sequential function method, was qualified and the influence of different possible signal qualities on the result of the reconstruction was investigated. Furthermore, the design and production of multi-depth temperature sensors was carried out. These sensors should have low manufacturing costs and dimensions with sufficient temporal and spatial resolution of the temperatures to be measured and thus offer the potential for extensive use in casting dies. Furthermore, in the first stage a test tool was designed and manufactured, which allows the integration and the use of the developed sensor technology for initial testing purposes. In the second phase, the chosen method for inverse calculation of the HTC was validated using a numerical model where the HTC was known in advance. Furthermore, the suitability, as well as the accuracy of the manufactured temperature sensor, was validated by experiments at an electron beam machine. For this purpose, the surface of the multi-depth temperature sensor was heated by means of an electron beam and the surface temperature was measured with a pyrometer. By evaluating the synchronized measuring signals of the multi-depth temperature sensor and the pyrometer, the exact position of the individual measuring points could be determined using a finite element calculation. The third phase, which is presented in this publication, involves carrying out experiments with a test tool. The aim here was to obtain and evaluate measurement results using a real cast material and associated boundary conditions, such as maximum temperature, temperature gradients and shrinkage. A future step, which is a continuation of the present work and is not presented in the context of this publication, is the use in the context of an instrumented, industrial die casting die and the determination of corresponding component properties.

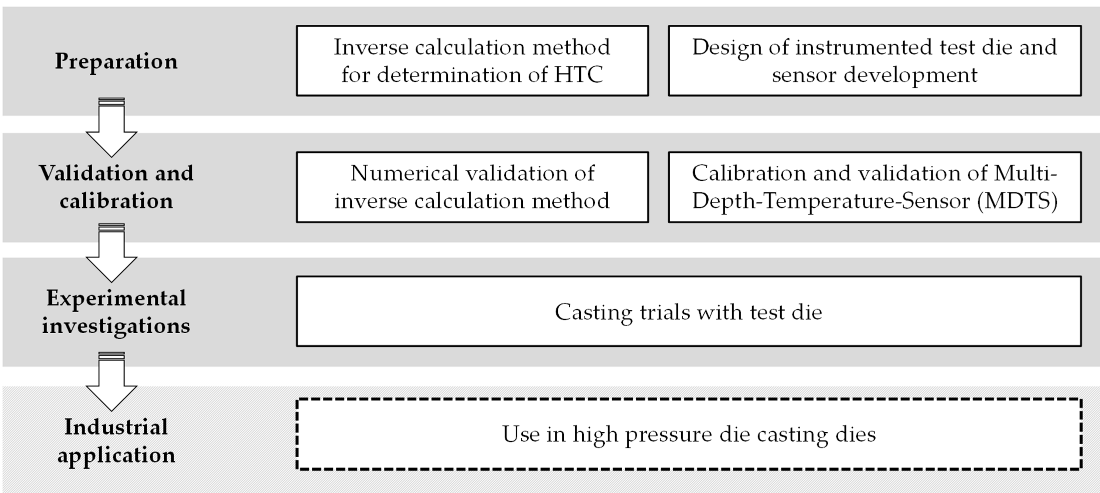

Figure 1. Main concept of the conducted work.

3. Steps Realization

3.1. Inverse Heat Conduction Problem and Estimation of the HTC

In some processes, such as die casting, where heat conduction problems occur, it is difficult to directly quantify the initial amount of heat flow at the exchange surface. This refers to the fact that the instrumentation at the die-casting surface is difficult to implement. However, it has been proven that from measurement points beyond the surface and within the heated body, the temperature profile can be recorded and later an inverse technique can be used to estimate the initial heat flow at the surface and the initial temperature [16]. The direct heat conduction problem in the 1-dimensional domain for a transient heat flow within a semi-finite body of length L is modeled in Figure 2 and expressed by the diffusion Equation (1a) and the different boundary conditions (1b–e).

$$\rho C(T)\frac{\partial T(x,t)}{\partial t} = \frac{\partial}{\partial x}\left(\lambda(T)\frac{\partial T(x,t)}{\partial x}\right);\ (x,t) \geq 0 \tag{1a}$$

where ρ (density), C (mass specific heat) and λ (thermal conductivity) are the temperature-dependent material properties of the body.

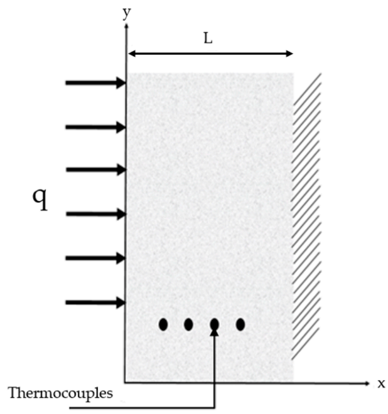

Figure 2. Model of 1-D heat conduction system.

i The initial temperature of the slab is considered to be a uniform value:

$$T(x,0) = T_0;\ t = 0 \tag{1b}$$

ii At the surface, the slab is subjected to a transient heat flux $q(t)$ and the temperature is suddenly changed:

$$-\lambda(T)\frac{\partial T(0,t)}{\partial x} = q(t);\ t \geq 0 \tag{1c}$$

iii The opposite surface of the slab is insulated:

$$\lambda(T)\frac{\partial T(L,t)}{\partial x} = 0;\ t \geq 0 \tag{1d}$$

iv The temperature inside the slab can be given by:

$$T(x,t) = Y + \varepsilon;\ (x,\ t) \geq 0 \tag{1e}$$

where Y is the experimental measured temperature data. To solve the problem, minimization by the method of least squares is widely used in order to determine the surface temperature T by means of the measured temperatures Y at different locations within the body as follows:

$$F = \sum_{i=1}^{n} \sum_{j=1}^{l} (Y_{i,j} - T_{i,j})^2 \to \min \tag{2}$$

where n represents the number of observations and l represents the number of sensors or the positions of the thermocouples. The index i corresponds to the time step index and j to the position index. On this basis many inverse techniques were developed, such as the Tikhonov regularization [17]. A very efficient method, however, has been used in particular to solve nonlinear heat conduction problems and has been applied to the die casting process by many researchers [10,14,16–18]. This is the method of nonlinear function specification (FSM), known as Beck's method. The FSM is sequential in nature and calculates the heat flux density function by estimating a discrete segment, starting with an initial estimate of q [19]. It also has the advantage of using a very small computational time step for more precision in the calculation. The estimated quantity of q on each small segment should be constant for a certain future time step designed by r [19]. The final solution for determining the heat flux density function q is therefore represented by Equation (3), where M is the current time step.

$$q_M = q_{M-1} + \frac{\sum_{i=1}^{r} \sum_{j}^{l} X_{qij}(Y_{i,j} - T_{i,j})}{\sum_{i=1}^{r} \sum_{j}^{l} {X_{qij}}^2} = q_M + \Delta q_M \tag{3}$$

The quantity in Equation (4) represents the sensitivity coefficient, which defines the temperature response, at one measurement point, to a step change in the heat flux:

$$X_{q_{i,j}} = \frac{\partial T_{i,j}}{\partial q_M} \tag{4}$$

In a final step, after calculating the heat flux density q, the HTC can be calculated using Equation (5) below:

$$HTC = \frac{q}{T_{cast} - T_{die}} \tag{5}$$

where T_{cast} corresponds to the temperature of the casting and T_{die} is the retrieved temperature value of the die using the inverse method. A MATLAB (R2017a) algorithm was used to calculate the HTC, considering the temperature-dependent material properties of the die material used.

3.2. Validation of the Method

To evaluate the method used, a simple one-dimensional heat conduction model was created in ANSYS (2020R1). The initial temperature of the solid was set to 25 °C and the ambient temperature to 720 °C. Temperature-dependent material data of the used hot work steel (H11) were considered for the solid. Furthermore, the simulation model was given time-dependent courses of the heat transfer between ambient temperature and body, see Figure 3a,b. The respective courses of the HTC reflect the characteristic behavior of the heat transfer at the interface between the cast component and the die during the solidification of a cast component. In order to avoid the risk of over-optimizing the reconstruction algorithm, two different HTC curves were selected, each of which is characteristic for fast or slow changes in the heat transfer at the surface. Virtual temperature sensors were defined in the model, whose positions correspond to the determined positions of the real multi-depth temperature sensor. In this way, it was also possible to show whether the number of measuring points of the multi-deep temperature sensor and their depth positions were adequate for a reliable reconstruction of the HTC (see Sections 3.3 and 3.4). In both cases, the heat conduction problem was solved and the calculated transient temperatures at the four individual measuring points were extracted and used for the reconstruction of the HTC. The assumed calculation time steps for the inverse calculation are set 1.5 times higher than the sampling time of the simulation and the used number of future times is $r = 3$.

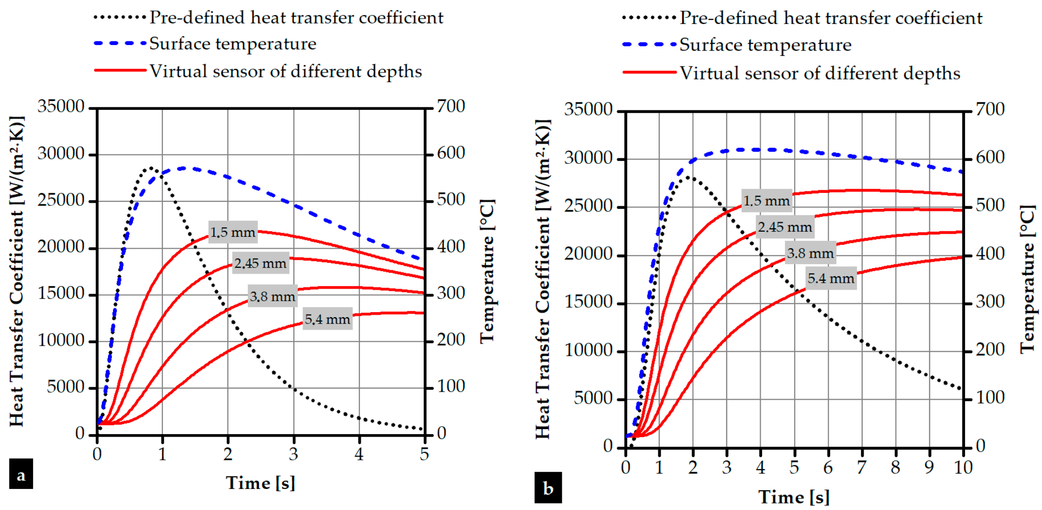

Figure 3. Given data for the simulation: (**a**) first run case; (**b**) second run case.

Figure 4a,b visualize the calculation results for the course of the reconstructed HTC and the predefined HTC for both cases. As shown in the figures, the reconstructed HTC was found to be in good agreement with the given curve for both cases, in terms of peak value, absolute values, and time offset. The peak-to-peak evaluation shows that this deviation is 0.05 s.

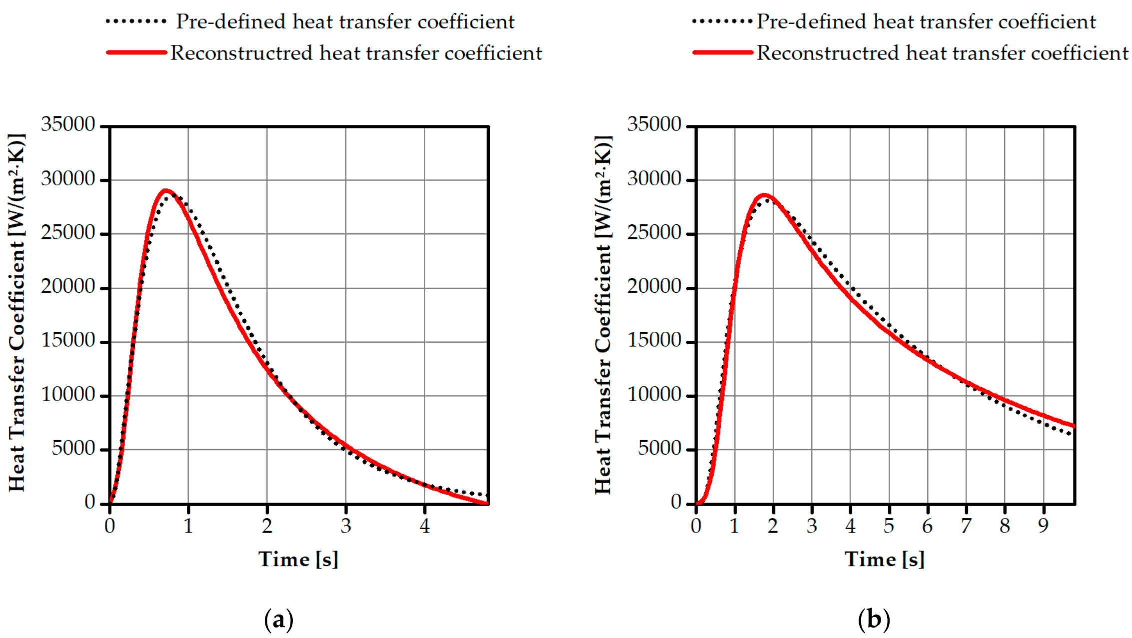

Figure 4. Temperature profiles and the corresponding reconstructed heat transfer coefficient (HTC): (**a**) first run case; (**b**) second run case.

3.3. Sensor Manufacturing

The presence of more than one temperature measurement point in the tool depth allows a better reconstruction of the heat transfer coefficient. Therefore, it was necessary to design and manufacture a temperature sensor that allows the temperature inside the tool to be measured at different distances from the die surface. The sensor should also assure long-term resistance to the process conditions, especially the temperature of the melt as well as mechanical loads. Furthermore, it should be compatible with the data acquisition hardware used for the project and should be usable by other systems for further applications. This goal was realized on the basis of simple electronics and joining technology and with a low complexity of the production steps. The design concept consists of two bodies joined by electron beam welding. Inside the sensor, a total of four type *K* thermocouples were integrated at close distances to the surface. The necessary pocket for the thermocouples was designed to be as small as possible in order to minimize distortion of the temperature field due to the recesses. The bodies were then further processed by machining to form a cylindrical body with additional geometric and functional features. The sensor was made of the same material (H11 tool steel) as the die and was hardened and tempered to 40 ± 1 HRC according to the usual procedure (annealing, quenching, and then two tempering stages). By using the same tool material, errors during reconstruction due to different thermal conductivities of the materials used were avoided. At the same time, there is good knowledge of the temperature-dependent thermal conductivity [20] of the hot work tool steel H11. By heat-treating to a hardness of 40 HRC, on the one hand the mechanical stability of the sensor was ensured. On the other hand, this hardness also ensured a reliable machining process and the compliance with shape and position tolerances, since hardness steps in the transition to the weld seam were avoided. Thermocouples from OMEGA Engineering (Deckenpfronn, Germany) were used and brought into direct contact with the substrate by local welding to ensure a fast response time with regard to the rapid changes in heat transfer at the interface between the component and the tool. The thermocouples used are 5TC-TT-KI-30 with a weld joint, and accuracy of DIN class 1. Each thermocouple has a diameter of 0.25 mm (with 30 AWG) and is protected against high temperatures by Kapton tape insulation [21]. The dimensions of the sensors are presented in Figure 5, with a schematic representation of the thermocouples inside. The numbers from 1 to 4 refer to the positions of the thermocouples according to their distance from the surface of the sensor. In addition, Figure 5b shows a cross-section of the sensor to illustrate the dimensions of the pocket in which the four thermocouples are integrated. Figure 6 shows the fully fabricated sensor. The arrangement of the thermocouples offers the advantage that several thermocouples can be integrated on one level, with each of them being positioned very close to the surface, adapted to the prevailing temperature gradient of the technical application. A possible disadvantage is the fact that the individual thermocouples are thus not arranged on a line perpendicular to the temperature gradient. This can be improved in other designs where the use of thin-film thermocouples is planned.

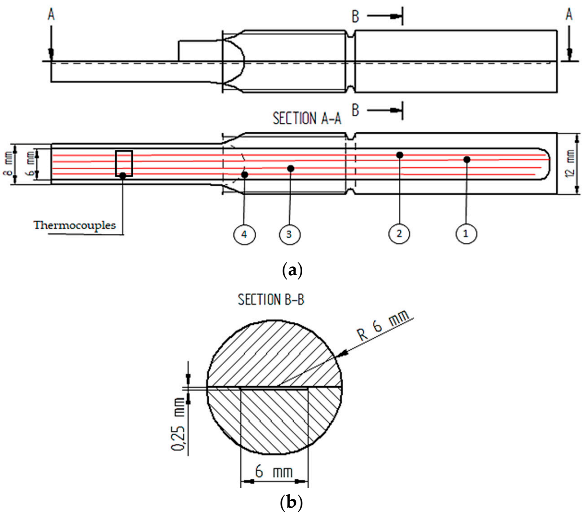

Figure 5. Geometry and dimensions of the sensor: (**a**) front view and cross-section of line A (**b**) cross-section of line B.

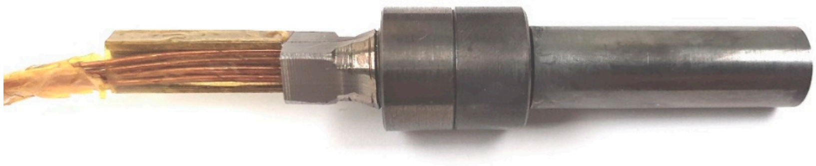

Figure 6. Manufactured multi-depth-temperature sensor.

The following section describes in detail the simulation-based approach to determine and validate the distance of the thermocouples from the surface.

3.4. Sensor Validation

An important step before implementing the multi-depth temperature sensor in practice is to verify two relevant features that are of great importance for a meaningful reconstruction of the HTC. These two features are the accuracy of the sensor's measurements and the efficiency in terms of time response. A sufficiently high accuracy of the HTC reconstruction requires that temperature measuring points are available at defined positions close to the surface and that the real existing positions also correspond to the positions assumed for the reconstruction. In fact, the exact position of the measuring point is usually only measured optically, whereby the exact position of the measured value generation for the weld spot on the thermocouple can often not be determined. The deviations in the range < 0.2 mm can lead to considerable errors in the reconstruction of the HTC, especially in the very near-surface area of the sensor (<2 mm), as calculations have indicated. For the investigations, the upper side of the sensor was exposed to a defined amount of heat generated by the electron beam gun inside the electron beam chamber. The temperature inside the sensor was measured on different levels by the thermocouples and at the same time the temperature of the surface was measured by a two-color pyrometer (M332) from Sensortherm GmbH integrated in the electron beam chamber. The measurement data were acquired using a script written in the LabVIEW development environment to ensure synchronization of both signals. The schematic test setup is shown in Figure 7.

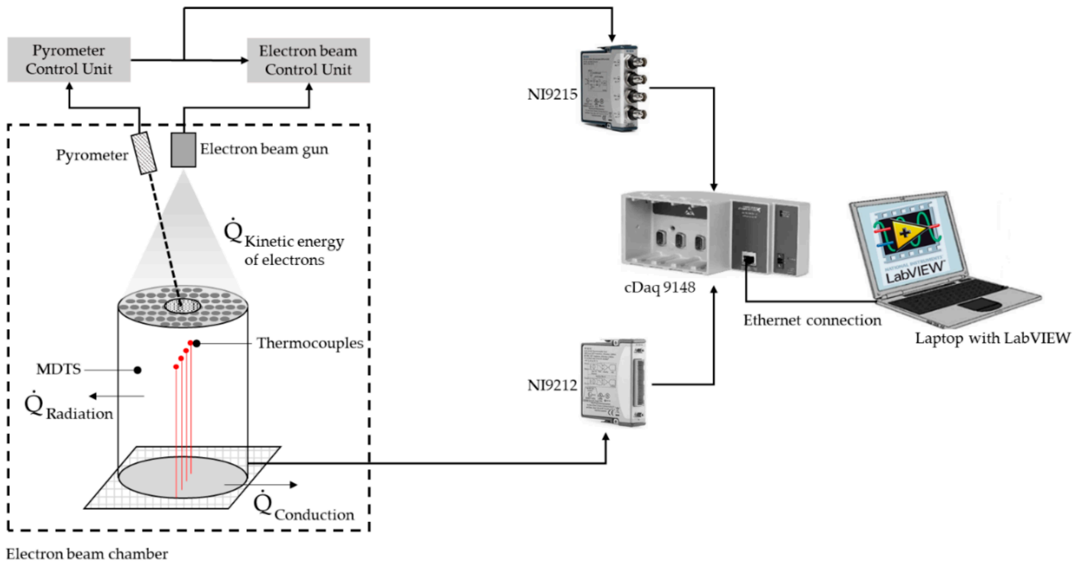

Figure 7. Experimental test setup for the validation of the sensor.

Figure 8 shows an example of the synchronized temperature curves of a multi-depth temperature sensor and a pyrometer for comparatively slow heating rates. High temperatures were deliberately chosen to verify the usability of the sensor at high temperatures. For casting processes, however, more dynamic heating rates are relevant. Thus, in further experiments, a higher energy of the electron beam was used to achieve higher heating rates (see Figure 8b). An evaluation of the time offset of the respective maxima (pyrometer and MDTS-1) resulted in a difference of approximately 0.13 s to the first near-surface temperature sensor, which is considered, as an initial time response guess, a very good value considering the measurement signal of the ratio pyrometer, which can be assumed to be without delay. Thus, it could be shown that measurements up to 750 °C at the surface of the pyrometer are possible. The sensor allows a fast reaction to abrupt changes in surface temperature. As mentioned above, a necessary step for a meaningful reconstruction of the heat transfer coefficient is the determination and validation of the exact positions of the thermocouples inside the sensor. The calibration and evaluation of the sensor was performed for two different heat flux densities and associated heating rates. On the one hand, relatively long heating and cooling cycles (Figure 8a) as well as for short-term temperature variations (Figure 8b), as they occur with similar dynamics in casting processes. For the purpose of determination and validation, the simulation environment ANSYS was used, in which the finite element method was applied for a thermal model to calculate the transient temperature fields inside the sensor body. The same boundary conditions as in the experimental step were implemented and the temperature measured by the pyrometer was now defined as a transient temperature boundary condition at the surface. The model was solved and the calculated temperature curves at discrete points were compared with the real measured temperature curves. The Newton–Raphson method was used to vary the position of the virtual thermocouple until a minimum of deviation between the calculated and experimentally determined result was found. The procedure was applied for long and short-term measurements and for all four measuring positions. In each case, three different cycles were chosen for the determination of the exact depths, and the average of the retrieved positions has been considered. For the long-term evaluation, only the heating cycles were used in order to avoid any secondary effects regarding the difference in boundary conditions between the simulation and the real experimental environment. The evaluation of the results made it possible to identify the corresponding positions {−1.5; −2.45; −3.8; −5.4 mm} in the case of long-term evaluation (Figure 9a), and {−1.5; −2.5; −3.95; −5.8 mm} for the short-term evaluation (Figure 9b) for the four thermocouples (MDTS1 to MDTS4). The procedure also allowed the depth determined in each case to be indicated with a mean value and a standard deviation; details can be found in Table A1.

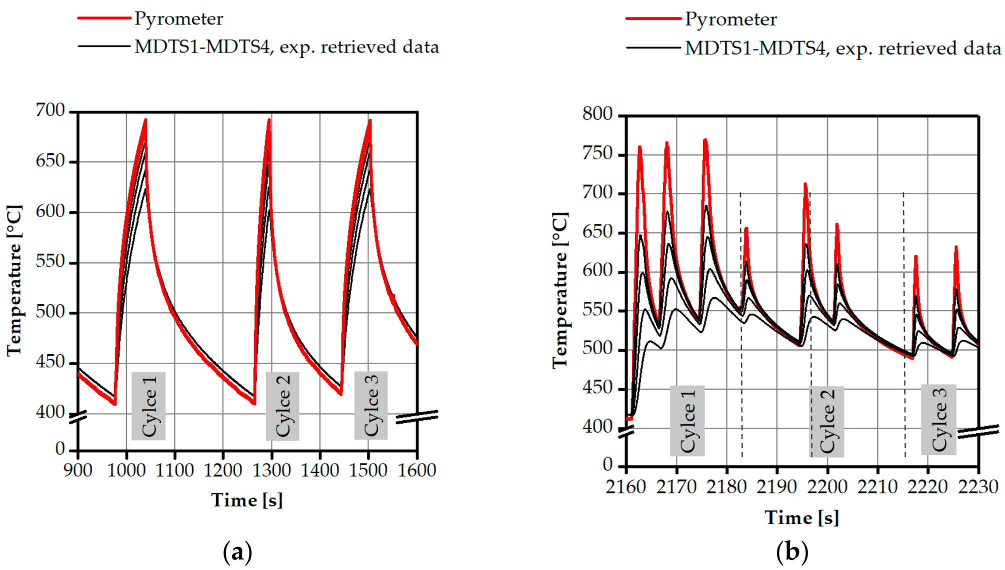

Figure 8. Experimental results: (**a**) long-time heating cycles measurements; (**b**) short-time cycles measurements.

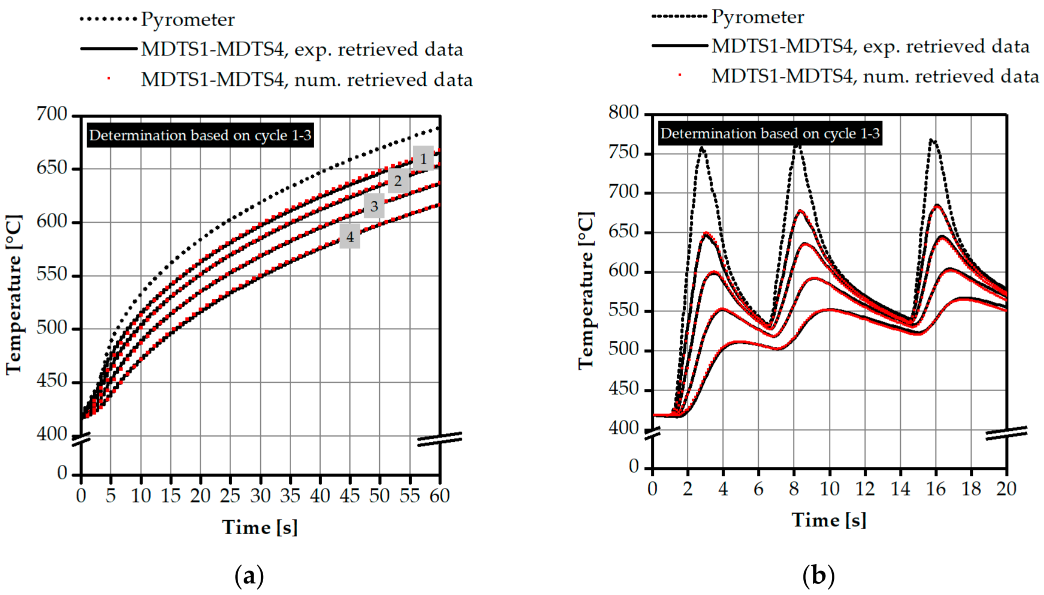

Figure 9. Comparison of the experimental and the finite element calculations: (**a**) long-term determination; (**b**) short-term determination.

3.5. Evaluation of the Uncertainty of the HTC Reconstruction

The presence of uncertainty of the exact locations of the thermocouples has an influence on the reconstruction of the HTC. For this reason, the uncertainty of the HTC also was evaluated, based on the reconstruction performed in Section 3.2 for the first run case for the retrieved positions in case of a long-term evaluation. The evaluation was done for different sets of thermocouples' positions (Table 1). The selection of the different sets was based on evaluating three measurements regions; for positions in the interval of ± 0.5 mm for the retrieved depths in case of long-term measurements (Set 1 and Set 2), for more distant locations (Set 3 and 4) and, finally, for very close positions to the surface (Set 5 and 6). For all these cases, the HTC results were compared to the reconstructed HTC determined for long-term measurements as a reference signal. Moreover, the HTC was also calculated for the short-term range, considering the retrieved locations for this case, where the results are very close to the long-term reconstruction results with a very small error of 0.5% (Figure 10). The computation results in Figure 10 allowed defining a maximum error that does not exceed 2% for Set 1 and 2, which is considered a small error. For Set 5 and 6, which are very close to the surface, lower HTC values were determined with a difference of 8.2% to the maximum reference value. Set 3 represents the depths at which the thermocouples are considered far from the surface, a higher HTC with a difference of 6.5% from the reference was reconstructed.

Table 1. Used depths for the evaluation of the uncertainty (values in mm).

Evaluation Sets	Thermocouples Depths			
	MDTS1	**MDTS2**	**MDTS3**	**MDTS4**
Long-term	−1.5	−2.45	−3.8	−5.4
Set 1	−1.5 − 0.5	−2.45 − 0.5	−3.8 − 0.5	−5.4 − 0.5
Set 2	−1.5 + 0.5	−2.45 + 0.5	−3.8 +0.5	−5.4 + 0.5
Set 3	−1.5 × 1.5	−2.45 × 1.5	−3.8 × 1.5	−5.4 × 1.5
Set 4	−3	−4	−5	−6
Set 5	−0.5	−1	−1.5	−2
Set 6	−0.25	−0.5	−0.75	−1

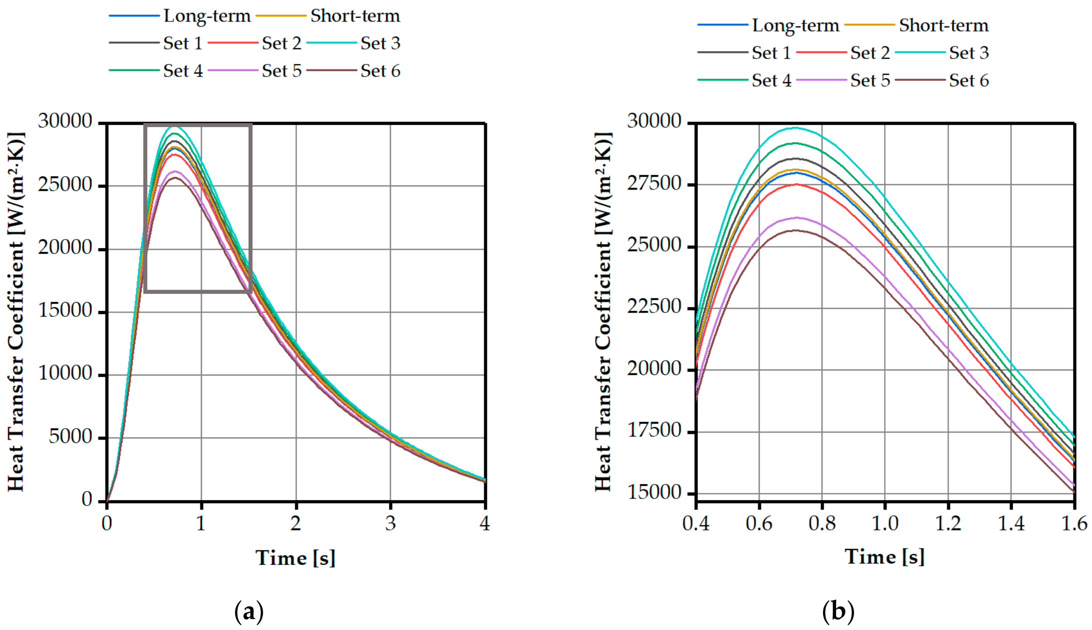

Figure 10. Uncertainty of the reconstructed HTC to variant thermocouples' depths: (**a**) full scale; (**b**) enlarged scale.

The temperature-dependent thermophysical properties also have a considerable influence on the HTC reconstruction. Hence, the uncertainty of the HTC regarding the variation of the thermal conductivity and the specific heat was evaluated. The conventional values of the thermophysical properties of the steel H11 (see Table A2) were varied by ±10%. The results of the calculation in Figure 11 show that the error of the signal does not exceed 5.1% when the values are increased by 10%. A decrease of 10% leads to a maximum error of 10% of the reconstructed HTC.

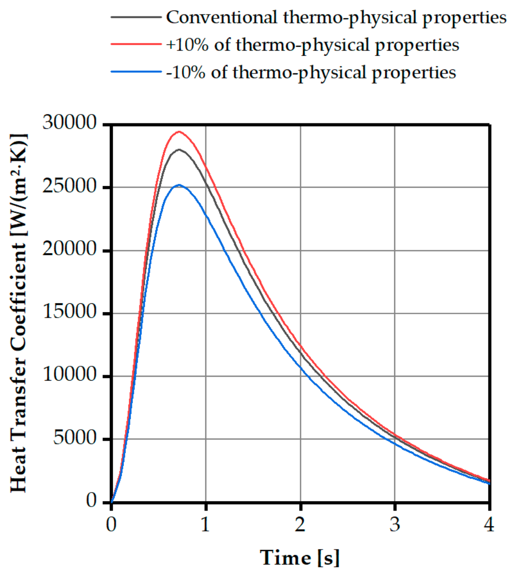

Figure 11. Uncertainty of the reconstructed HTC to a variation of the thermos-physical properties.

3.6. Design of the Instrumented Test Tool

The basic idea behind the design of the instrumented tool is the fact that embedded sensors in the die and on the direct contact surface between the die and the casting make it possible to record real-time data in throughout the casting process, thus enabling the cooling conditions of the melt and the onset of gap formation to be recorded more accurately. The actually designed test tool is equipped with three sensors: the multi-deep temperature sensor, a pyrometer to measure the temperature of the die or the temperature of the casting and a displacement sensor that allows us to evaluate the shrinkage of the part by measuring the distance from the die surface during the solidification phase until complete solidification. The aspect of shrinkage is not discussed in this paper, as it is more useful in the real process under high pressure conditions in the cavity. The tool is characterized by a modular design, with each sensor inserted in a single block and all blocks having the same dimensions. This principle is applied to the real tool in further steps, as it offers more flexibility to replace the sensors individually, e.g., in case of damage, or to configure their positions within the die instead of replacing the complete die. The dimensions of the die are (150 × 50 × 125) mm^3 with a cavity depth of 25 mm. The arrangement of the sensor positions is shown in Figure 12. To protect the pyrometer against high pressure and high temperature of the melt, five Al_2O_3 sapphire windows [22], with a thickness of 1 mm each, are employed.

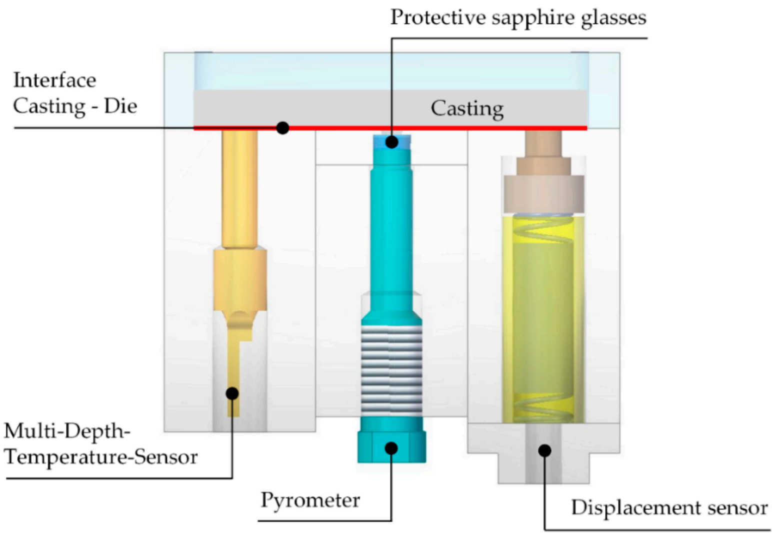

Figure 12. Design of the instrumented test tool.

4. Experimental Results and Discussion

4.1. Experimental Conditions and Setup

The casting tests with the designed test tool were carried out at the institute. This made it possible, in a first step, to validate the effective function of the entire test set-up before the measuring sensor technology was transferred to the real casting process. Many casting series were carried out successively in order to gain insights into the sustainability and behavior of the sensors and the influence of the temperature of the melt on the sapphire windows. The alloy used in the casting tests was AlSi10Mg, which has the chemical composition in (weight percent) given in Table A3. The tool was manufactured from the material X38CrMoV5-1 (H11). Table A2 shows the various temperature-dependent thermal properties of hot work tool steel. The data acquisition was ensured by a complete hardware setup from National Instruments. The die temperature was recorded with a sampling rate of 95 S/sec/channel and a resolution of 24 bit. The integrated pyrometer is the IGAR 12-LO IMPAC from Advanced Energy (LumaSense Technologies GmbH), which measures according to the two-color ratio principle [23]. It operates at a temperature value from 300 °C and runs at a baud rate of 19.2 kBd, which enables data to be acquired at high speed and with greater accuracy.

During the first casting tests, it has been noticed that the melt temperature measurements are switched off directly after few seconds of pouring. This can be explained by the fact that the molten aluminum alloy changes its state from liquid to solid, which implies changes of the emissivity. This physical behavior can cause a problem when measuring with the pyrometer in ratio-mode due to changing emissivity in a different way on both channels. Moreover, using the IGAR 12-LO IMPAC pyrometer, which has a wavelength of (1.52 µm/1.64 µm), a measurement on aluminum alloy leads to a very low signal level, as this alloy has a very low emissivity in the wavelength range of this pyrometer. When the alloy changes state from liquid to solid, the signal strength goes below the switch-off level of the pyrometer, leading to wrong measurements. To remedy this problem, in order to adapt the existent pyrometer to be adequate to measure the aluminum alloy temperature, the level signal strength of the pyrometer was adjusted so that the wavelength supports the changing emissivity of the melt and does not break off during measurements. In addition, a simple calibration test was carried out to ensure that the correct temperature was recorded by the pyrometer over the temperature range to be measured. Within the scope of this experiment, the alloy used (approximately 300 g) was heated in a furnace to different, predefined temperatures (a respective holding time of 15 min was considered). At each holding point, the temperature of the melt was measured both by thermocouple and pyrometer. The results of this procedure are shown in Figure 13. The quantified error in percentage over all the trials is 2.1%, which shows a good agreement between the measurements. However, less error is expected, since the nature of this experiment required that the melt had to be taken outside the furnace and measure directly the temperature using the pyrometer.

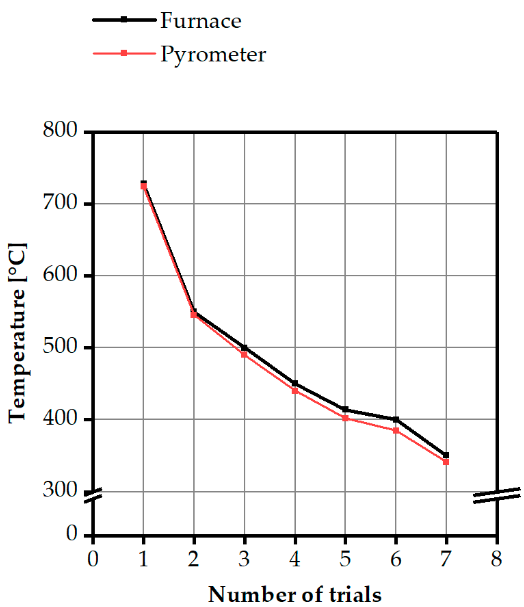

Figure 13. Calibration of the pyrometer.

4.2. Process Description and Results

The experimental procedure is described in Figure 14, using an equal amount of melt of 100 g for each casting cycle.

During the filling phase (step 1), which was measured due to the manual filling of 4 s, the molten melt was poured directly onto the sapphire windows (pyrometer). This results from the high peak, which was recorded at casting temperatures of approximately 700 °C for all casting series carried out (Figure 15). At the same time, however, the multi-depth temperature sensor did not detect the maximum die temperature, so that the die starts to heat up to record a first peak value for the first two seconds and then rises to a maximum peak value of about 225 °C. The main reason is the flow of the liquid metal from the center of the cavity to the end of the cavity wall and back to the inner sides, immediately after the filling phase and during the first seconds of the solidification phase (step 2). During the solidification phase of about 90 s, the melt began to solidify and lift off from the ends of the mold cavity. The evaluation of the HTC during the solidification phase took place in a time interval of 25 s. At the end of this phase, the completely solidified casting has a shape as shown in step

3 of the process; the uncovered shape may be the cause. Figure 15 represents the measurements of temperatures profiles for the die and cast for the first casting cycle.

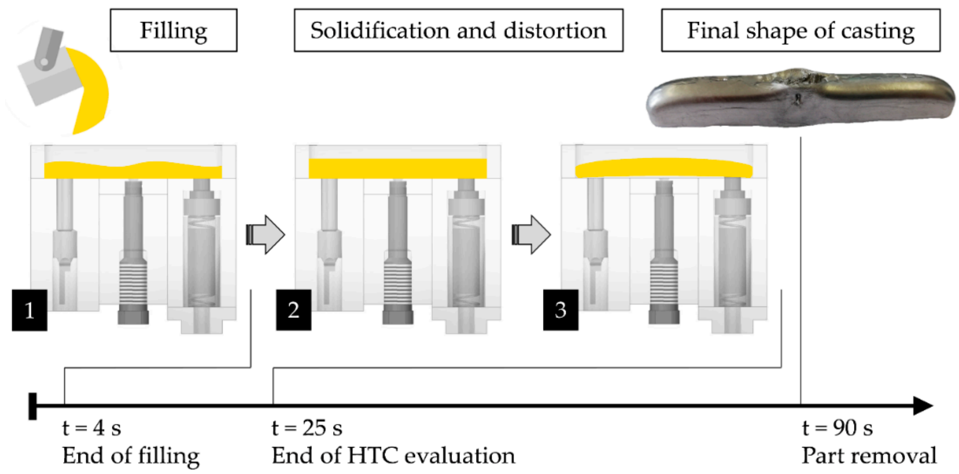

Figure 14. Description of the experimental process.

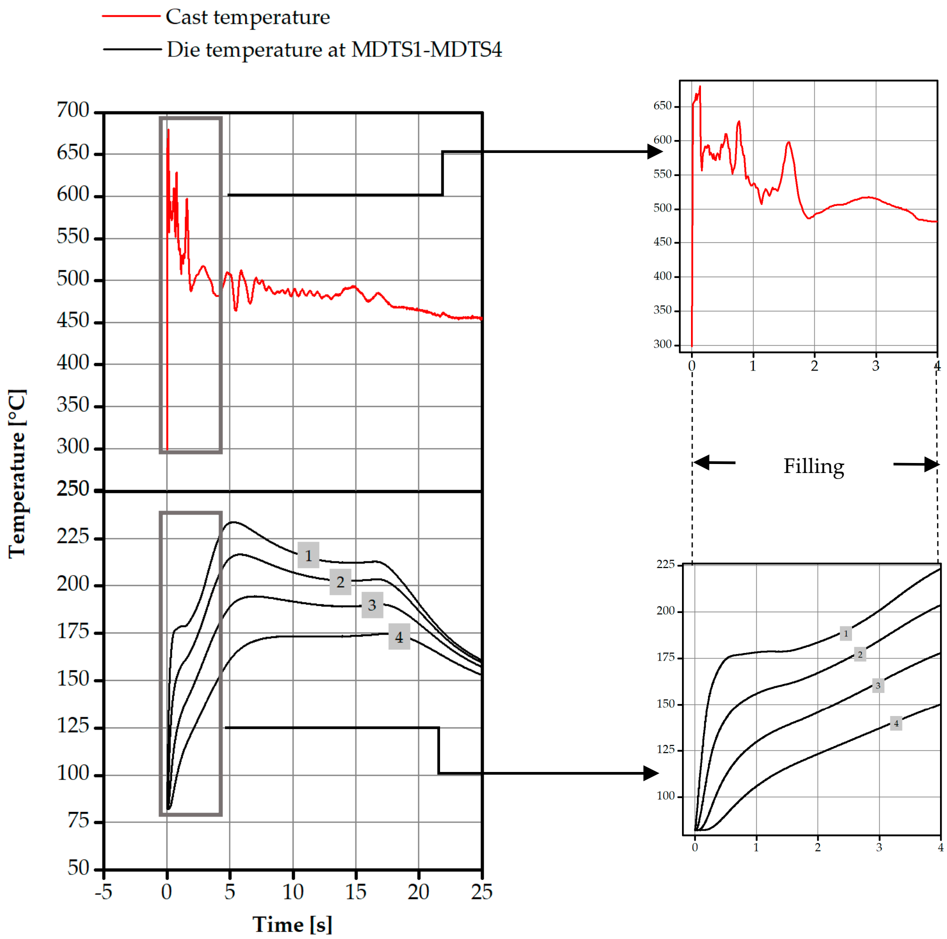

Figure 15. Experimental temperature profiles for the die and the cast for cycle 1.

4.3. Determination of the HTC

Although the presence of this important noise on the recorded temperature of the cast, which is mainly caused at the first 5 s by the filling of the melt and after that by solidification stage, it was possible to reconstruct the HTC history without any filtering of the input data using the inverse method. Figure 16 shows the estimated HTC profiles for the three casting cycles in a time interval of 25 s.

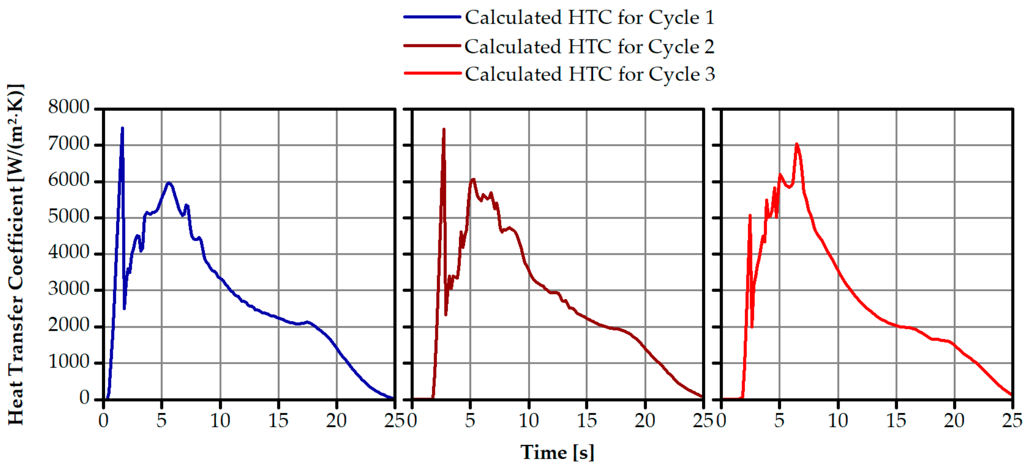

Figure 16. Calculated heat transfer coefficient (HTC) for Cycle 1–Cycle 3.

From the reconstructed HTC profiles, it can be seen that comparable values are found for the three casting experiments. This can be interpreted by the fact that the same experimental conditions were maintained during the entire series.

For cycles 1 and 2, an HTC peak value of 7500 W/(m^2·K) was determined for a range temperature values of the die between 170 °C and 225 °C right at the beginning of filling for the cast series due to the high temperatures of the melt. When the liquid is completely poured, its distribution inside the cavity becomes uniform, ensuring perfect contact between the cast and the die. Here, the heat exchange from the cast surface to the die body is increasing, which then results at the beginning of solidification on the second peak of the calculated HTC, which shows an average value of 6000 W/(m^2·K) for almost all casting series. At a further stage, when the cast starts to cool down and shrink rapidly, an air gap gradually begins to form between the two surfaces, causing the HTC to decrease rapidly. Generally, the HTC values are not high compared to the real process, since there is no high pressure applied on the cast. Furthermore, it was found that the small differences in the initial starting temperatures of the die-casting mold for the casting series did not lead to large differences in the calculated HTCs. Compared to the first cycles, some differences can be seen on the reconstructed HTC for cycle 3. The reconstruction results show that at the beginning of the filling phase the HTC for cycle 3 is lower by 2500 W/(m^2·K), compared to cycle 1 and 2. Moreover, after the filling phase, the recorded second peak is higher by 1000 W/(m^2·K). These results can be explained by the differences in the measured temperature profiles between cycles 1–2 and cycle 3 (see Figure A1) due to the nature of the conducted experiments. The reconstructed HTCs are affected by the noise on the measured temperature signal from the pyrometer. For this, Figure A2 gives additional information about the reconstructed heat flux for cycle 1 as an example. The result shows a smooth signal compared to HTC, since it is based on the temperature data of the die. The highest heat flux value determined at pouring time is about 180 kW/(m^2); then it reaches a second peak of around 110 kW/(m^2) once the cavity is completely filled with melt. After that, it starts to decrease slowly due to solidification.

5. Conclusions and Outlook

In this work, an instrumented test die dedicated for casting applications was presented, which embeds three different sensors that are directly exposed to the contact surface of the die and the cast. This tool allows us to track the thermal and the physical behavior of the cast in real time. During the conducted experimental castings series, the test tool, as well as the sensors, showed a robust performance in terms of the stable measurements and the good resistance to the high temperature of the melt. The collected experimental data by means of this tool and the associated data acquisition system were used for the determination of the interfacial heat transfer coefficient between the cast and the die using an inverse method. The inverse calculation of the HTC shows that the values are comparable for the presented casting series and shows a value of 6000 W/(m^2·K) after the filling process.

In future research, further studies should first be carried out on the multi-deep temperature sensor to evaluate its time response. Furthermore, different sensor designs, which include different arrangements as well as sensor types (e.g., thin-film sensor thermocouples) are in the foreground. In addition, the present instrumentation is used to perform numerous experiments taking into account different cavities and thus cooling rates and HTCs. In the future, a closed cavity will be used, which is more closely oriented to the solidification and distortion boundary conditions of real cast components. As the main motivation of this work is to use the integrated sensors for the HPDC process, an instrumented real die casting tool is designed and applied afterwards. Here, the real process conditions have to be considered, especially with regard to the high internal pressure applied to the mold. Furthermore, the course of gap formation during solidification between mold and casting is evaluated with the integrated displacement sensor and calculated in parallel by simulation-based approaches. In the future, this procedure should allow a much better process control, which detects deviating heat flows of the cast part due to a different tool temperature control, an inhomogeneous application of the mold release agent, as well as other deviating casting parameters. At the same time, the process data obtained allows for a better component and process design.

Author Contributions: Conceptualization, Y.K. and S.M.; methodology, Y.K.; validation, Y.K. and T.S.; writing—original draft preparation, Y.K.; writing—review and editing, S.M.; supervision, K.D.; project administration, S.M.; funding acquisition, S.M. and K.D. All authors have read and agreed to the published version of the manuscript.

Funding: This research project was funded by Volkswagen AG as part of the Open Hybrid Lab Factory (OHLF) research initiative, which aims at an application-oriented research into production technologies and new materials for economical and multifunctional lightweight design in the field of hybrid lightweight structures. The authors would like to express their gratitude for the financial support provided.

Conflicts of Interest: The authors declare no conflict of interest.

Appendix A

Table A1. Considered Depths of the thermocouples.

Long-Term Determination	Short-Term Determination	Mean Value	Standard Deviation
−1.5	−1.5	−1.5	0
−2.45	−2.5	−2.475	0.03536
−3.8	−3.95	−3.875	0.10607
−5.4	−5.8	−5.6	0.28284

Table A2. Thermal material properties of the H11.

Temperature (°C)	C_p (J·kg^{-1}·K^{-1})	λ (W·m^{-1}·K^{-1})	ρ (kg·m^{-3})
20	440.9	26.5	7800
100	466.1	27.3	7776
200	490.9	28.2	7746
300	511	28.7	7716
400	529.2	29	7687
500	548.5	28.9	7645
600	582.3	28.4	7600
700	622.8	28.2	7550

Table A3. Chemical composition of the Aluminum alloy AlSi10Mg.

Element	Al	Si	Fe	Cu	Mn	Mg	Ni	Zn	Pb	Sn	Ti
Percentage	Balance	9–11	0.055	0.1	0.45	0.20–0.45	0.05	0.10	0.05	0.05	0.15

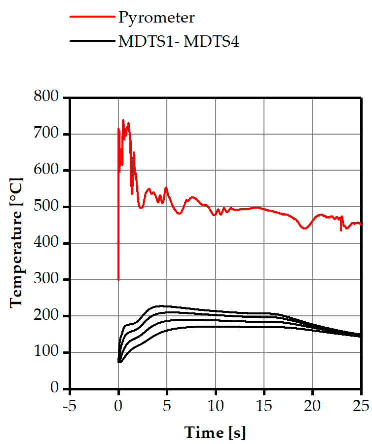

Figure A1. Cast and die temperature for cycle 3.

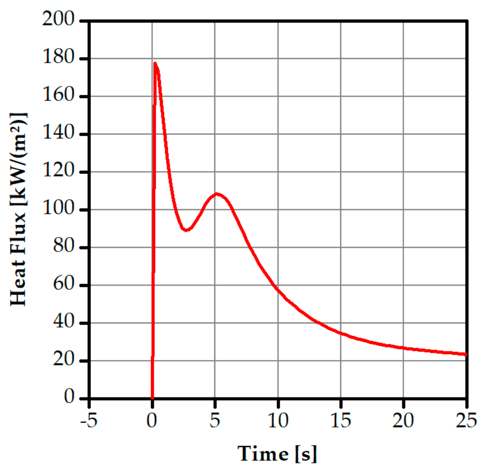

Figure A2. Reconstructed heat flux for cycle 1.

References

1. Winkler, M.; Kallien, L.; Feyertag, T. Correlation between process parameters and quality characteristics in aluminum high pressure die casting. *NADCA*. Available online: https://www.researchgate.net/publication/283726141_Correlation_between_process_parameters_and_quality_characteristics_in_aluminum_high_pressure_die_casting (accessed on 1 September 2020).
2. Dour, G.; Dargusch, M.; Davidson, C. Recommendations and guidelines for the performance of accurate heat transfer measurements in rapid forming processes. *Int. J. Heat Mass Transf.* **2006**, *49*, 379–390. [CrossRef]
3. Kobliska, J.; Ostojic, P.; Cheng, X.; Zhang, X.; Choi, H.; Yang, Y.; Li, X. Rapid Fabrication of Smart Tooling with Embedded Sensors by Casting in Molds Made by Three Dimensional Printing. *Int. Solid Free. Fabr. Symp.* **2005**, *42*, 468–475.
4. Tiedemann, R.; Pille, C.; Dumstorff, G.; Lang, W. Sensor Integration in Castings Made of Aluminum—New Approaches for Direct Sensor Integration in Aluminum High Pressure Die Casting. *Key Eng. Mater.* **2017**, *742*, 786–792. [CrossRef]
5. Ageyeva, T.; Horváth, S.; Kovács, J.G. In-Mold Sensors for Injection Molding: On the Way to Industry 4.0. *Sensors* **2019**, *19*, 3551. [CrossRef] [PubMed]

6. Tian, L.; Guo, Y.; Li, J.; Xia, F.; Liang, M.; Bai, Y. Effects of Solidification Cooling Rate on the Microstructure and Mechanical Properties of a Cast Al-Si-Cu-Mg-Ni Piston Alloy. *Materials* **2018**, *11*, 1230. [CrossRef] [PubMed]
7. Snopiński, P.; Król, M.; Tański, T.; Krupińska, B. Effect of cooling rate on microstructural development in alloy ALMG9. *J. Therm. Anal. Calorim.* **2018**, *133*, 379–390. [CrossRef]
8. Hosseini, V.A.; Shabestari, S.G.; Gholizadeh, R. Study on the effect of cooling rate on the solidification parameters, microstructure, and mechanical properties of LM13 alloy using cooling curve thermal analysis technique. *Mater. Des.* **2013**, *50*, 7–14. [CrossRef]
9. Jamaly, N.; Haghdadi, N.; Phillion, A.B. Microstructure, Macrosegregation, and Thermal Analysis of Direct Chill Cast AA5182 Aluminum Alloy. *J. Mater. Eng. Perform.* **2015**, *24*, 2067–2073. [CrossRef]
10. Yongyou, C.; Zhipeng, G.; Shoumei, X. Determination of the metal/die interfacial heat transfer coefficient of high pressure die cast B390 alloy. *IOP Conf. Ser. Mater. Sci. Eng.* **2012**, *33*, 012010.
11. Hamasaiid, A.; Dargusch, M.S.; Davidson, C.; Loulou, T.; Dour, G. A Model to Predict the Heat Transfer Coefficient at the Casting-Die Interface for the High Pressure Die Casting Process. *AIP Conf. Proc.* **2008**, *907*, 1211.
12. Vasileiou, A.N.; Vosniakos, G.-C.; Pantelis, D. Determination of local heat transfer coefficients in precision castings by genetic optimisation aided by numerical simulation. *Proc. IMechE Part C J. Mech. Eng. Sci.* **2015**, *229*, 735–750. [CrossRef]
13. Aksoy, B.; Koru, M. Estimation of Casting Mold Interfacial Heat Transfer Coefficient in Pressure Die Casting Process by Artificial Intelligence Methods. *Arab. J. Sci. Eng.* **2020**, *31*, 45. [CrossRef]
14. Cao, Y.; Guo, Z.; Xiong, S. Determination of interfacial heat transfer coefficient and its application in high pressure die casting process. *China Foundry* **2014**, *11*, 9.
15. Pille, C. Smart systems integration. In Proceedings of the 4th European Conference & Exhibition on Integration Issues of Miniaturized Systems-MEMS, MOEMS, ICs and Electronic Components, CD-ROM, Como, Italy, 23–24 March 2010.
16. Zhang, Y.; Wen, Z.; Zhao, Z.; Bi, C.; Guo, Y.; Huang, J. Laboratory Experimental Setup and Research on Heat Transfer Characteristics during Secondary Cooling in Continuous Casting. *Metals* **2019**, *9*, 61. [CrossRef]
17. Dhodare, A.; Ravanan, P.M.; Dodiya, N. A Review on Interfacial Heat Transfer Coefficient during Solidification in Casting. *IJERT* **2017**, *6*, 464–467.
18. Dargusch, M.S.; Hamasaiid, A.; Dour, G. An Inverse Model to determine the Heat Transfer Coefficient and its Evolution with Time during Solidification of Light Alloys. *Int. J. Nonlinear Sci. Numer. Simul.* **2008**, *9*, 275–282. [CrossRef]
19. Beck, J.V. Nonlinear estimation applied to the nonlinear inverse heat conduction problem. *Int. J. Heat Mass Transf.* **1970**, *13*, 703–716. [CrossRef]
20. Kaschnitz, E.; Hofer, P.; Funk, W. Thermophysikalische Daten eines Warmarbeitsstahls mit hoher Wärmeleitfähigkeit. *Giesserei* **2010**, *97*, 42–45.
21. OMEGA. Available online: www.omega.de (accessed on 1 September 2020).
22. Edmund Optics. Available online: https://www.edmundoptics.com/p/125mm-diameter-uncoated-sapphire-window/34724/ (accessed on 1 September 2020).
23. Advanced Energy. Impac ISR 12-LO and IGAR 12-LO Series. Available online: https://www.advancedenergy.com/ (accessed on 1 September 2020).